RSC Advances

PAPER

View Article Online
View Journal | View Issue

Cite this: *RSC Adv.*, 2025, **15**, 33657

Engineered MCM-48 and heteropolyacid based hybrid nano-drug delivery systems for controlled release of metformin hydrochloride for diabetes mellitus treatment

Debatrayee Dasgupta and Anjali Patel *

Received 16th May 2025
Accepted 2nd September 2025

DOI: 10.1039/d5ra03450g

rsc.li/rsc-advances

In the present study, hybrid drug delivery systems based on 12-tungstophosphoric acid and nano MCM-48 were developed to improve the bioavailability and dosing frequency of an antidiabetic drug, metformin hydrochloride. The role of 12-tungstophosphoric acid as a functionalizing and capping agent was also studied. An *in vitro* release study was carried out at pH 1.2 and pH 7.4 at 37 °C to see the effect of pH, followed by a release kinetic study and the comparison of release profiles with a marketed drug, Glycomet-250. Further, a dissolution study was carried out using a type II USP dissolution apparatus. Taking into consideration the anticancer activity of metformin hydrochloride, an MTT assay using HepG2 cells was performed, and it was found that the customised system can dramatically reduce hyperglycaemic conditions and exhibit potential activity towards HepG2 cells.

1. Introduction

Metformin hydrochloride (MTF), classified as a class III drug in the Biopharmaceutics Classification System (BCS), is a biguanide anti-hyperglycaemic drug that is often used in the treatment of diabetes mellitus type II (DMT2).[1] MTF operates by improving the insulin sensitivity, boosting the lipid metabolism, inhibiting the hepatic gluconeogenesis, decreasing the risk of developing fatty liver, and minimising the body weight and cardiovascular problems.[2,3]

In 1932, the association between diabetes and cancer was discovered accidently; however, the current clinical research demonstrates a two-way relationship between diabetes and cancer, and it shows that diabetic patients are prone to developing cancer.[4] However, interestingly, recent studies have suggested a link between the hypoglycaemic drugs and cancer. Therefore, according to clinical, epidemiological, and preclinical studies, MTF could potentially be able to stop the development of cancer cells. The mechanism behind the anticancer effects of MTF has been explored. A review of the literature reveals that several animal model studies claim that the use of MTF alone or in combination with radiation therapy can reduce tumour growth. MTF often inhibits mammalian target of rapamycin (mTOR) activity by activating ATM (ataxia telangiectasia mutated), LKB1 (liver kinase B1), and AMPK (AMP-activated protein kinase), which in turn inhibit cell growth and protein synthesis.[5–9]

However, MTF, on the other hand, has poor intestinal absorption owing to its high water solubility. Due to its poor pharmacokinetics, including a low bioavailability of 50–60% as well as a short half-life of 3–4 h, a high dose (1.5–3 g day^{-1}) is frequently required, which causes adverse effects including lactic acidosis and gastrointestinal (GIT) irritation. Consequently, frequent administration of substantial amounts of MTF results in decreased patient compliance and a higher incidence of adverse effects such as anorexia, diarrhoea, vomiting, and nausea.[10,11] As a result, numerous nanotechnological approaches have been explored that improve drug bioavailability and minimize the demand for repeated administration.

Over the last two decades, nanomedical breakthroughs have improved the approach of developing mesoporous silica nanoparticle (MSN)-based drug delivery systems (DDSs), which significantly enhance the drug delivery efficacy due to their known advantages.[12] Furthermore, due to the abundance of active sites of surface silanol groups (Si–OH) in MSNs, significant efforts have been made to modify the surface of MSNs with active moieties, such as antibodies and peptides, and specific ligands, such as mannose, hyaluronic acid and folic acid.[13–18] Thus, literature reveals that the surface of MSNs has been functionalized using organic moieties, and hence, it would be interesting to use an inorganic moiety for functionalization. In this direction, heteropolyacids (HPAs) are one of the excellent candidates due to their known advantages.

HPAs represent an emerging class of inorganic metal oxides, which over the last decades demonstrated promising biological activities by virtue of their great structural diversity which includes size, surface charge distribution, acidity and redox potential. They are oxoanions of transition metal ions, such as V, Mo, W, Nb, and Pd, and in the series of different types of

Department of Chemistry, Faculty of Science, The Maharaja Sayajirao University of Baroda, Vadodara, 390002, India. E-mail: anjali.patel-chem@msubaroda.ac.in

HPAs, the Keggin-type HPAs are stable and easy to synthesis. It is reported that the Keggin-type HPAs exhibit antibacterial, antiviral, anti-protozoal, anticancer, and antidiabetic properties, which resulted in anticipation for their application as bioinorganic medications. A review of the literature reveals that 12-tungstophosphoric acid (TPA), a Keggin type of HPA, has been reported to have various potential biological applications.[19–22] Studies on diabetic mice and rats have previously focused on polyoxotungstates and the tungsten metal alone, and in small animals, tungstate has been shown to restore pancreatic beta cell activity and increase insulin secretion.[23] TPA was therefore chosen as the functionalizing agent to functionalize the surface of MSNs from the perspective of medicinal chemistry.

Thus, this work aims to reduce the severe side effects of MTF and enhance its efficacy *via* a developed drug delivery system based on 12-tungstophosphoric acid (TPA)-functionalized MCM-48 nanoparticles (nMCM-48), as shown in Fig. 1. Three DDSs were developed and compared to see whether TPA acts better as a capping or as a functionalizing agent. The developed DDSs were characterized by various physiochemical techniques. An *in vitro* release study was carried out in both the Simulated Body Fluid (SBF) and the Simulated Gastric Fluid (SGF), and the obtained release profile was compared to that of the marketed available formulation Glycomet-250 using a USP type II dissolution apparatus. Various models including the zero-order, first-order and Higuchi were studied to assess the drug release kinetics and mechanisms. Finally, the anticancer potential of MTF against the liver cancer cell line (HepG2) through the MTT assay was evaluated.

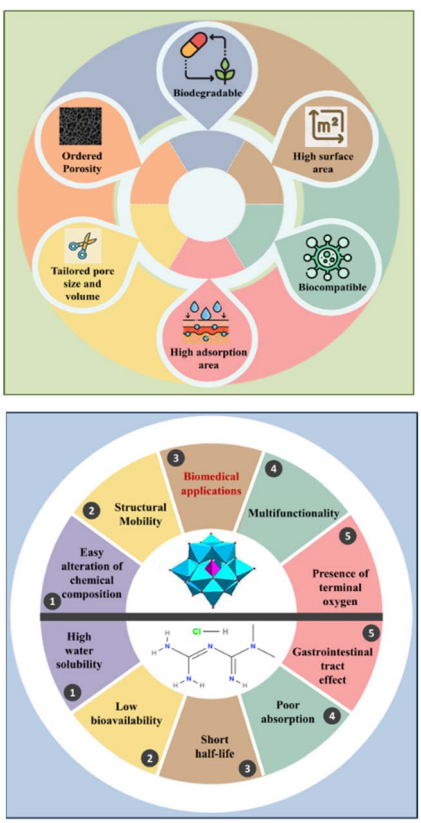

Fig. 1 Illustration of the unique properties of nMCM-48 and heteropolyacid as well as its advantages as a drug delivery system to overcome the limitations of metformin hydrochloride.

2. Experimental section

2.1. Chemicals and reagents used

12-Tungstophosphoric acid, tetraethylorthosilicate (TEOS), ethanol, and liquor ammonia (25%) were procured from Merck. Metformin hydrochloride (MTF) was received from Sigma Aldrich. Cetyltriethylammonium bromide (CTAB) was purchased from Lobachemie, Mumbai. Glycomet-250, a commercially accessible formulation of MTF (each tablet with an active dose of 250 mg of the medication), was obtained from medical store. All the chemicals acquired were of the A. R. grade and utilized without any further purification.

Preparation of the release medium:

Two different release media were prepared, namely, simulated body fluid (SBF) and simulated gastric fluid (SGF), representing the pH of gastric and human blood plasma. Therefore, SBF was prepared by dissolving 400 mg of NaCl, 10.7 mg of KCl, 72.5 mg of Na_2HPO_4, and 12.5 mg of KH_2PO_4 in 250 mL of distilled water, while SGF was prepared by dissolving 6.2 g of concentrated HCl in 1000 mL distilled water.

2.2. Synthesis of 12-tungstophosphoric acid (TPA) functionalized nMCM-48

nMCM-48 was synthesised following the procedure previously reported by our group.[24,25] Briefly, CTAB (2.4 g) was added to distilled water (50 mL) and allowed to dissolve completely at 35 °C. To this, ethanol (50 mL) and 25% liquor ammonia (15.4 mL) were added. The mixture was then stirred for a duration of 15 to 20 min. Additionally, TEOS (3.4 g) was added dropwise, and the mixture was stirred for 2 h. Following filtration, distilled water rinsing, room-temperature drying, and 6 h of calcination at 550 °C, a white material was obtained. The resulting white material was designated as nMCM-48.

2.3. Functionalization of nMCM-48 with 12-tungstophosphoric acid (TPA)

nMCM-48 was functionalized with TPA by an incipient wet impregnation method, as previously reported by our group.[24,25] First, 1 g of nMCM-48 was functionalized with 30% of TPA (0.3 g in 30 mL of distilled water) and then dried at 100 °C for 10 h. The obtained material was designated as TPA/nMCM-48

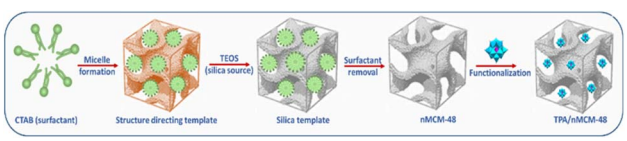

Scheme 1 Schematic illustrating the synthesis of nMCM-48 and its subsequent functionalization using TPA.

(Scheme 1). The synthesis yield of TPA/nMCM-48 was found to be 92.3%.

2.4. Loading of MTF into the nanocarriers

MTF was loaded using a solvent immersion technique. nMCM-48 (20 mg) were ultrasonically dispersed in 20 mL solution of MTF in distilled water (MTF concentration = 1 mg mL^{-1}) for 10 min to ensure uniform dispersion. Following that, the suspension was then stirred for 24 h at room temperature. After a period of 24 h, the drug loaded nanoparticles were isolated *via* ultracentrifugation and the supernatant was collected separately, while the solid drug-loaded nanoparticles were washed with acetone twice to remove the untrapped MTF. Finally, the particles were air-dried and the obtained material was designated as MTF/nMCM-48. Similarly using the same method, MTF was loaded into TPA/nMCM-48 and the obtained material was designated as MTF/TPA/nMCM-48 (Scheme 2).

The amount of MTF loaded was measured by collecting the supernatant solution. The amount of unloaded MTF in the supernatant solution was determined spectrophotometrically using a PerkinElmer Lambda 35 UV-Visible spectrophotometer at a wavelength of 234 nm. Therefore, the % entrapment efficiency was calculated for MTF/nMCM-48 and MTF/TPA/nMCM-48, respectively, using the following equation:

$$\%\ \text{Entrapment efficiency} = \frac{(E_c - E_s)}{E_c} \times 100$$

where E_c indicates the concentration of MTF taken, while E_s indicates the concentration of MTF in supernatant.

2.5. Capping of MTF/nMCM-48 by TPA

In order to assess the effect of TPA on the release rate of the drug, another system was synthesized by capping MTF/nMCM-48 using TPA. To put it briefly, a 30% aqueous solution of TPA (0.3/30 g mL^{-1} distilled water) was used to cap 1 g of MTF/nMCM-48, and the obtained material was designated as TPA/MTF/nMCM-48.

2.6. Characterization of the synthesized nanocarriers

A Shimadzu instrument (IRAffinity-1S) was used to record the FTIR spectra in the range of 400–4000 cm^{-1}. Using a hydraulic pellet press, the samples were compressed to create pellets using the KBr pellet method. Using a transmission electron microscope, JEOL TEM apparatus (Model-JEM 2100), the surface morphology of the synthesised materials was recorded. With a 200 kV electron beam, the TEM micrographs of the materials were recorded using a carbon-coated copper TEM grid. The SEM analysis was carried out using the Model-JSM 5610 LV EDS-SEM analyzer. Using a Mettler Toledo Star SW 7.01 instrument in a nitrogen atmosphere, the samples were subjected to thermogravimetric differential thermal analysis (TG-DTA) at temperatures between 50 and 800 °C, at a flow rate of 2 mL min^{-1} and a heating rate of 10 °C per minute. A comprehensive characterization study of TPA/nMCM-48 and nMCM-48 has been incorporated in our previous research work. However, FT-IR spectroscopy, SEM, TEM, and TGA are included in the current work for comparison as well as for reader's convenience.

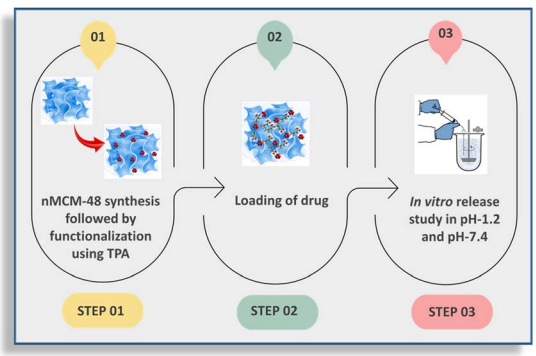

Scheme 2 Schematic of step-wise synthesis and loading of drug-loaded materials.

2.7. *In vitro* evaluation of release profiles

To investigate the *in vitro* release, a soaking method was employed. Two extreme pH values (pH-7.4, SBF and pH-1.2, SGF) were employed as releasing media to represent the extreme pH conditions encountered in the human body, namely, the highly acidic environment of the stomach and the neutral physiological pH of the systemic circulation. Then 5 mg of MTF/nMCM-48 was suspended in 10 mL of release medium (SBF or SGF), and the mixture was constantly stirred at 37 °C. To assess the quantity of MTF released, aliquots were obtained from the release media at various time intervals. An equivalent amount of completely fresh release media was used to replace each sample that was removed. The amount of MTF released by the other systems was estimated by using the same methodology. The amount of MTF released in each of the release media was measured using a PerkinElmer Lambda 35 UV-Visible spectrophotometer at a wavelength of 234 nm. The relationship between cumulative MTF release against time was plotted.

2.8. Dissolution study using USP paddle apparatus

The evaluation of *in vitro* dissolution was carried out following the guidelines established by the USP. Using a USP type-II dissolution apparatus (Rotating Peddle), the *in vitro* dissolution studies were carried out. Both pH 7.4 and pH 1.2 were used as the dissolving media, which were maintained at 37 °C ± 0.5 °C. At predetermined intervals, a 3 mL aliquot was removed and replaced with an equal volume of the release medium. The drug content was measured in the samples using a UV spectrophotometer (PerkinElmer Lambda 35 UV-Visible spectrophotometer) set to 234 nm.

2.9. *In vitro* cytotoxicity study protocol

The MTT assay is a simple colorimetric assay developed by Mosmann to measure the metabolic (mitochondrial) reductive competence of cells, which is an indicator of cell viability.[26] Cytotoxicity assays are typically applied for *in vitro* cytotoxicity evaluations due to their easy handling and low cost. To evaluate the cytotoxicity of the synthesised compounds against the

HepG2 cell line, which is employed as a model for human hepatocellular carcinoma, the modified method of the colorimetric MTT assay was used in this study for cytotoxicity testing. To sum up it briefly, HepG2 cells were grown in Dulbecco's modified Eagle's medium (DMEM), which was enriched with 1% Himedia antibiotic/antimycotic solution and 10% foetal bovine serum (FBS). The growth environment was maintained in a CO_2 incubator at 37 °C with a 5% CO_2 level. The cells were cultured until reaching confluence, separated using Himedia's 0.25% trypsin–EDTA solution, plated in 96-well plates at a density of 10 000 cells per well, and then incubated for an additional 24 h to promote cell adhesion. After incubation, the cells were exposed to various doses of the synthesized material (25, 50, 100, and 200 μg mL^{-1}) for a duration of 24 h.

Immediately after completion of the treatment, a 3-(4,5-dimethylthiazol-2-yl)-2,5-diphenyltetrazolium bromide or MTT solution (5 mg mL^{-1}) was added to the medium containing the compounds, and the mixture was incubated for an additional 4 h. Following the incubation period, formazan crystals were dissolved in 100 μL of DMSO, and the absorbance was assessed using an ELISA plate reader set at 570 nm. The relative percent viability was computed using the following formula, with the viability of the untreated control being considered as 100%:

$$\%\ \text{Cell viability} = \frac{(\text{test samples absorbance})}{(\text{control absorbance})} \times 100$$

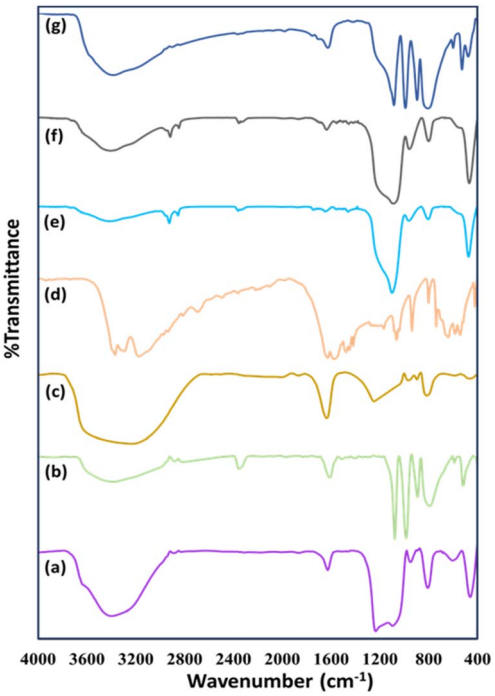

Fig. 2 FT-IR spectra of (a) nMCM-48, (b) TPA, (c) TPA/nMCM-48, (d) MTF, (e) MTF/nMCM-48, (f) MTF/TPA/nMCM-48, and (g) TPA/MTF/nMCM-48.

3. Results and discussion

3.1. Solid-state characterization of the synthesized nanocarriers

Fig. 2 and Table 1, respectively, indicate the major FT-IR bands and frequencies for each material (nMCM-48, TPA, TPA/nMCM-48, MTF, MTF/nMCM-48, MTF/TPA/nMCM-48, and TPA/MTF/nMCM-48), along with their corresponding FT-IR spectra. The successful synthesis of nMCM-48 is illustrated by the characteristic peak for Si–O–Si symmetric stretching. Successful functionalization with TPA is confirmed by the fingerprint bands, which indicate that the primary structure of TPA remains unchanged even after impregnation.[24,25] Two prominent bands, corresponding to the secondary and primary amines, were seen at 3371 cm^{-1} and 3291 cm^{-1} in the FTIR spectra of pure MTF.[27] A distinctive band, attributed to C–N stretching, was observed at 1457 cm^{-1}. In case of MTF/nMCM-48, the peak at 471 cm^{-1} associated with the Si–O bending vibration suggests the interaction of the drug with the silica framework of nMCM-48. FTIR studies revealed that fundamental peaks of the MTF corresponding to C–N and C=N stretching at 1636 and 1457 cm^{-1} were retained in MTF/nMCM-48 with a slight shift in the peaks from 935, 1063 and 2821 to 958, 1094 and 2854 cm^{-1}, showcasing the successful loading of MTF into nMCM-48. The FT-IR spectrum of MTF/TPA/nMCM-48 shows the presence of all the corresponding characteristic peaks at 469, 787, 1092, 1640 and 2856 cm^{-1}, showing a strong interaction between MTF and TPA/nMCM-48 with structural retention of TPA even after loading. Similarly, TPA/MTF/nMCM-48 exhibits a shift in the characteristic peaks of TPA at 890 and 987 cm^{-1}, along with changes in the peaks at 1079, 1622, 471 and 593 cm^{-1}, corresponding to the distinctive peaks of MTF and nMCM-48. These shifts confirm the successful capping with TPA.

The TEM images of nMCM-48, TPA/nMCM-48, MTF/nMCM-48, and MTF/TPA/nMCM-48 are captured at different magnifications, as shown in Fig. 3. The TEM images of the synthesised nMCM-48 effectively illustrate the nanoporous architecture of the material by depicting porous channels as alternate black and white stripes. It displays the uniformly sized, well-organized pore networks (Fig. 3(a and e)). As shown in Fig. 3(b and f), darker spheres were seen in the case of TPA/nMCM-48 compared to nMCM-48. This suggests that TPA has been equally distributed throughout the pores. Additionally, loading with the drug demonstrates consistent dispersion of MTF in the case of MTF/nMCM-48 (Fig. 3(c and g)) and MTF/TPA/nMCM-48 (Fig. 3(d and h)), with no morphological modification or aggregation. This is further supported by the SEM images.

The SEM images (Fig. 4) show that all the particles have a spherical morphology with a uniformly distributed particle size. Even after the introduction of TPA, the SEM images of TPA/nMCM-48 show no apparent morphological change, confirming the fine dispersion of TPA. Furthermore, TPA/MTF/nMCM-48 shows no discernible morphological change following TPA capping, suggesting its uniform dispersion after capping.

The TGA and DTA curves for nMCM-48, TPA/nMCM-48, MTF, MTF/nMCM-48 MTF/TPA/nMCM-48 and TPA/MTF/nMCM-48 are shown in Fig. 5. The TGA plot of nMCM-48 reveals an

Table 1 FT-IR bands of the synthesized materials

Compound	Major peaks (cm^{-1})	Corresponding bands
nMCM-48	462	Si–O bending vibration
	578	Si–O–Si symmetric stretching
	1100, 1250	Si–O–Si asymmetric stretching
TPA	800	W–O
	987	W–O–W bending
	1088	P–O symmetric stretching
TPA/nMCM-48	810	W–O
	956	W–O–W bending
	1249	Si–O–Si asymmetric stretching
MTF	3371	Secondary amine
	3291	Primary amine
	3170	N–H stretching
	1624	C=N stretching
	1416	C–N stretching
MTF/nMCM-48	471	Si–O bending vibration
	1636	C=N stretching
	1457	C–N stretching
MTF/TPA/nMCM-48	467	Si–O bending vibration
	787	W–O
	960	W–O–W bending
	1640	C=N stretching
TPA/MTF/nMCM-48	593	Si–O–Si symmetric stretching
	987	C=O stretching
	1622	C=N stretching

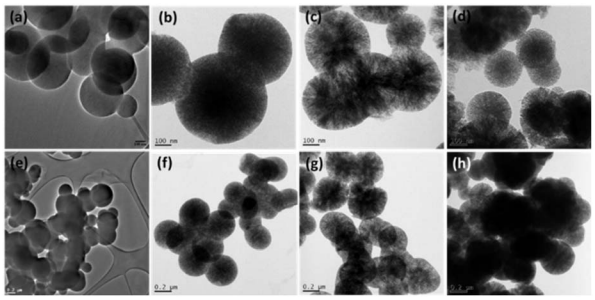

Fig. 3 TEM images of (a and e) nMCM-48, (b and f) TPA/nMCM-48, (c and g) MTF/nMCM-48 and (d and h) MTF/TPA/nMCM-48.

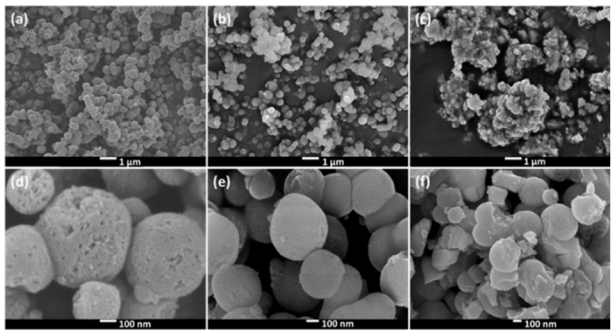

Fig. 4 SEM images of (a and d) MTF/nMCM-48, (b and e) MTF/TPA/nMCM-48 and (c and f) TPA/MTF/nMCM-48.

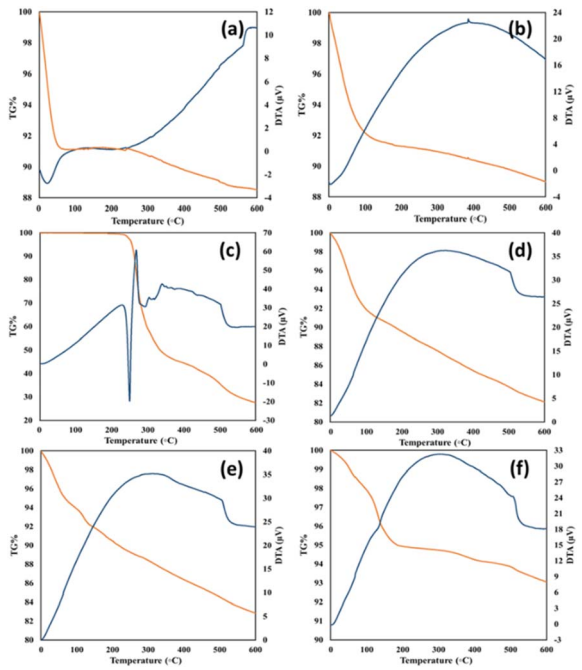

Fig. 5 TG-DTA plots of (a) nMCM-48, (b) TPA/nMCM-48, (c) MTF, (d) MTF/nMCM-48, (e) MTF/TPA/nMCM-48 and (f) TPA/MTF/nMCM-48.

initial weight loss of 8.9% up to 110 °C, which could be related to physically absorbed water molecules desorbing, and a final weight loss of less than 1% up to 400 °C, which is related to silanol groups in the nMCM-48 condensing. Adsorbed water is responsible for the first weight loss of 8.1% up to 115 °C displayed in the TGA of TPA/nMCM-48. Crystalline water molecules found in the Keggin unit are responsible for the second weight loss of 0.6% up to 200 °C. In contrast to MTF/nMCM-48 and MTF/TPA/nMCM-48, whose TGA curves display overall

losses of 15% and 18%, respectively, the TGA curve of MTF displays a loss of 65%. MTF/TPA/nMCM-48 results in a greater quantity of weight loss, which may be related to its increased drug entrapment efficiency. The DTA curves of MTF showed a typical sharp endothermic peak at 230 °C due to melting, which also corresponded to an endothermic volatilization of the hydrogen chloride molecule and the $C_4N_3H_7$ fragment. This was followed by an exothermic decomposition peak at 255 °C, which was attributed to the exothermic release of the H_4N_2 fragment.[28] For the MTF/nMCM-48 and MTF/TPA/nMCM-48, both the exothermic and endothermic peaks of MTF are diminished due to interaction with the carrier which shows the successful loading of the drug.

3.2. *In vitro* evaluation of release study

It was determined that MTF/nMCM-48 and MTF/TPA/nMCM-48 have entrapment efficiencies of 90% and 92%, respectively. Owing to the terminal oxygen bond present in TPA, a greater amount of the drug may be loaded, leading to better entrapment efficiencies, which justifies the higher amount of drug loading obtained in case of MTF/TPA/nMCM-48.

3.2.1. Effect of drug carrier ratio. The drug carrier ratio played an important role both in terms of amount of drug release and in terms of entrapment efficiencies as shown in Table 2. It was interesting to note that when the release study was carried out employing a drug carrier ratio (drug/carrier) of 1/1 and at pH 1.2, a very slow release was obtained, *i.e.*, at the end of 10 h, only 11.4% of the drug was released, as shown in Fig. 6. Eventually, it was thought to change the drug/carrier ratio from 1/1 to 0.5/1 to see the effect of ratio on the release rate. At the end of 10 h, 24.6% MTF was released and comparatively a faster release was obtained. Therefore, to further optimize the release study, the amount of drug taken for loading was decreased and a drug/carrier ratio of 0.1/1 was obtained. In this case, a substantial amount of drug release was obtained at the end of 10 h (67.4%), and therefore, the ratio 0.1/1 was optimised for carrying out the release studies. Moreover, upon changing the drug carrier ratio, there was a significant decrease in the amount of drug loading, respectively, upon decreasing the amount of drug. This trend was obtained because when the amount of drug is more, the pores are completely filled, and hence, it becomes difficult for the drug molecules to diffuse out due to less available space. Accordingly, when the amount of drug is decreased, it becomes easier for the drug molecule to diffuse out, and eventually, a faster release is obtained. The same trend was observed when the release study was carried out at pH 7.4, as shown in Fig. 7.

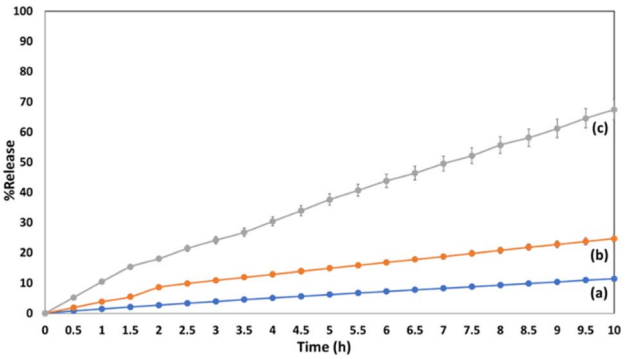

Fig. 6 Comparison of the *in vitro* release profiles using different drug carrier ratios: (a) 1 : 1 (b) 0.5 : 1 and (c) 0.1 : 1 at pH 1.2.

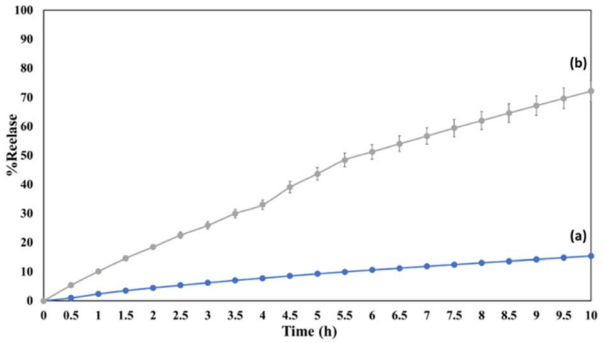

Fig. 7 Comparison of the *in vitro* release profiles using different drug carrier ratios: (a) 1 : 1 and (b) 0.1 : 1 at pH 7.4.

3.2.2. Effect of the pH and role of TPA on drug release. In order to see the effect of pH on release profile, the release study was also carried out in a simulated gastric fluid (SGF, pH-7.4) and compared with release profiles obtained in a simulated body fluid (SBF, pH 1.2), as shown in Fig. 8 and 9, respectively. According to the overall results for all three systems: MTF/nMCM-48, MTF/TPA/nMCM-48, and TPA/MTF/nMCM-48, a slower drug release was found at pH 1.2 compared to pH 7.4. This might be because the amino group of the MTF was protonated at pH-7.4, which means that the amino group is no longer present to form hydrogen bonds with the Si–OH group on the surface of the materials. As a result of this weakening of the MTF-material interaction, quicker release can be observed in SBF.

By comparing the release patterns of MTF from MTF/TPA/nMCM-48 and TPA/MTF/nMCM-48 at both pH 1.2 and pH 7.4, the effect of TPA as a functionalizing and capping agent was

Table 2 Effect of drug carrier ratio and entrapment efficiency on % release

Sr. no.	Materials	Drug: carrier	% Entrapment efficiency	% Release (after 10 h)
1	MTF/TPA/nMCM-48	1 : 1	99.0	11.4
2		0.5 : 1	96.0	24.6
3		0.1 : 1	92.0	67.4

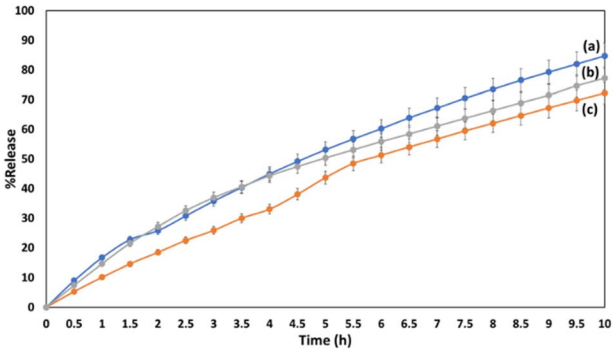

Fig. 8 *In vitro* release profiles of (a) MTF/nMCM-48, (b) MTF/TPA/nMCM-48 and (c) TPA/MTF/nMCM-48 at pH 7.4.

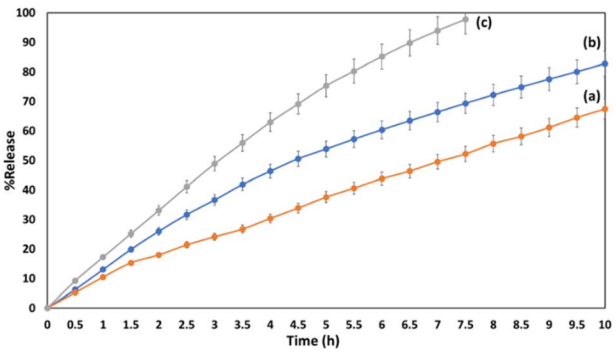

Fig. 9 *In vitro* release profiles of (a) MTF/nMCM-48, (b) MTF/TPA/nMCM-48 and (c) TPA/MTF/nMCM-48 at pH 1.2.

studied. According to the results, 43% of the drug was initially released from MTF/TPA/nMCM-48 and 50% of the drug was released from TPA/MTF/nMCM-48 at pH 7.4. After 10 h, 72% of the medication was released from the MTF/TPA/nMCM-48 system, whereas 77% was released from the TPA/MTF/nMCM-48 system, indicating a more rapid release. Comparably, at pH 1.2, initially, 37% of MTF is released from MTF/TPA/nMCM-48, while almost 75% of the drug is released from TPA/MTF/nMCM-48. After 7.5 h, 97% of the drug is released from TPA/MTF/nMCM-48 and only 67% is released from MTF/TPA/nMCM-48.

Thus, it is interesting to see that as compared to MTF/nMCM-48 and TPA/MTF/nMCM-48 systems, drug release occurs more slowly and efficiently in the MTF/TPA/nMCM-48 system. A potential explanation for the obtained pattern could be that the free terminal oxygen of TPA increases the possibility of a more favourable interaction with MTF resulting in more controlled release. This is presented in Scheme 3, the interaction involved between nMCM-48, TPA and the drug from the perspective of point of zero charge (PZC). The pH value (7.4) of nMCM-48 is higher than the PZC of silica, ~2–3, and hence the surface charge of nMCM-48 is negative.[29,30] As a result, upon functionalization, the negatively charged surface of nMCM-48 interacts with that of the available protons of TPA and the terminal oxygen of TPA will interact with the available protons of the drug after loading it.

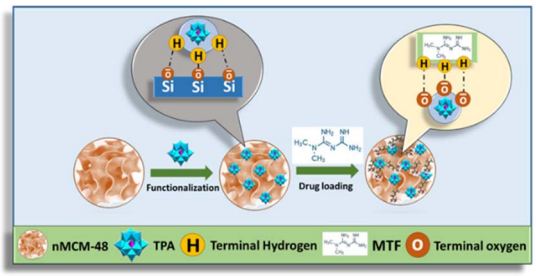

Scheme 3 Schematic depicting the various interactions involved between the drug, TPA and nMCM-48.

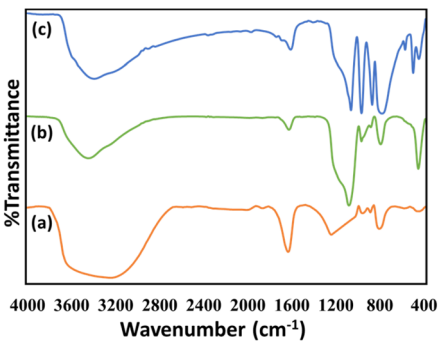

Fig. 10 FT-IR spectrum of (a) TPA/nMCM-48, (b) MTF/TPA/nMCM-48 after release study and (c) TPA/MTF/nMCM-48.

According to the release study, TPA only behaves as a functionalizing/capping agent, which was further confirmed by the FTIR spectra of MTF/TPA/nMCM-48 (Fig. 10), which was carried out after the release study. The spectra resemble that of TPA/nMCM-48 and TPA/MTF/nMCM-48 (Fig. 2), suggesting that TPA functions primarily as a functionalizing/capping agent and maintains its structural integrity during the drug release.

3.2.3. Comparison of the developed DDS with marketed available formulation. The superiority of the developed DDS, as shown in Table 3, was proven by comparing the release profiles of MTF/TPA/nMCM-48 with that of the marketed available formulation, Glycomet-250 (Fig. 11). The release profiles demonstrate that Glycomet-250 exhibits extremely rapid drug release, with nearly all of the drug being released by the end of the 2 h in both SBF and SGF. However, a significantly slower release is achieved with our developed DDS. It was observed that by the end of 10 h, almost 67% and 72% of the drug is released at pH 1.2 and pH 7.4, respectively. The observed trend in the

Table 3 Comparison of the release profiles

		% Release (37 °C, stirring condition, at the end of 10 h)	
Sr. no.	Formulations	pH-1.2	pH-7.4
1	Marketed formulation	96 (at 2.5 h)	95 (at 2.5 h)
2	MTF/TPA/nMCM-48	67	72

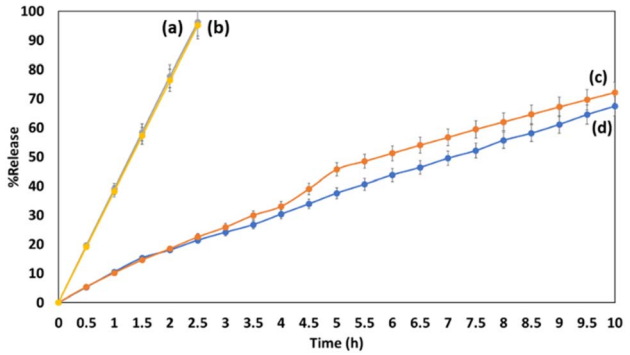

Fig. 11 Comparison of the *in vitro* release profiles of Glycomet-250 at (a) pH 7.4 and (b) pH 1.2, as well as the release profiles of MTF/TPA/nMCM-48 at (c) pH 7.4 and (d) pH 1.2.

data is due to the presence of the terminal oxygen bond on heteropolyacids, which is capable of holding the drug for an extended period of time and cause the drug to be released at a slower rate.

3.3 Dissolution study using a USP paddle apparatus

The rate of drug release is measured by a dissolution test. The underlying principle of this approach is that drugs must dissolve in the aqueous contents of the gastrointestinal tract prior to being absorbed. During the early phases of formulation development, *in vitro* dissolution testing offers recommendations for maximising drug release. In general, dissolution testing is essential to the development of new drugs since it helps with everything from formula optimisation to performance evaluation.[31–34]

Consequently, an *in vitro* dissolution study of MTF/TPA/nMCM-48 was carried out and the results were compared with that of Glycomet-250, the commercially available formulation. Upon analysing the release patterns (Fig. 12), it was observed that nearly the whole active amount of the drug was released from Glycomet-250 after 2.5 h in both SBF and SGF. However, only 99.7% of the medication was released from MTF/TPA/nMCM-48 after 10 h at pH 1.2 and 99.5% after 7.5 h at pH 7.4. Consequently, MTF/TPA/nMCM-48 showed a significantly slower and better release profile than Glycomet-250.

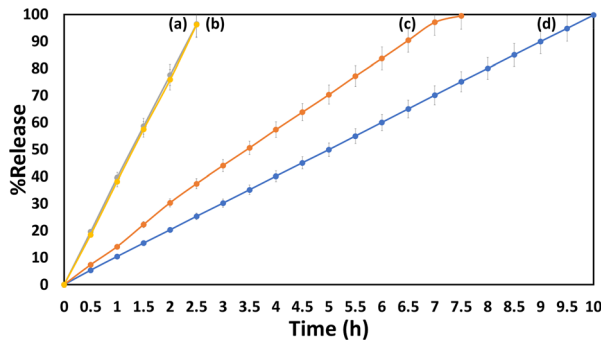

Fig. 12 Comparison of the *in vitro* dissolution release profiles of Glycomet-250 at (a) pH 7.4 and (b) pH 1.2, as well as the release profiles of MTF/TPA/nMCM-48 at (c) pH 7.4 and (d) pH 1.2.

Table 4 Comparison of the release profiles

Sr. no.	Systems	% Release (37 °C, stirring condition, at the end of 10 h) pH-1.2	pH-7.4
1	Marketed formulation	96.4 (at 2.5 h)	98.2 (at 2.5 h)
2	MTF/TPA/nMCM-48	99.7	99.5 (at 7.5 h)

Table 4 illustrates that the release profiles obtained from the *in vitro* release study are nearly identical to those obtained from the dissolution study conducted with a dissolution apparatus. This indicates that MTF/TPA/nMCM-48 behaves as a more effective drug delivery system for the controlled release of MTF than the commercially available formulation Glycomet-250. This is substantiated by the fact that TPA functions as a functionalizing agent, binding to the drug through the terminal oxygen atoms and causing a delayed release.

3.4. Release kinetics models

The dissolution data were subjected to release kinetics study. Different mathematical models have been used to analyze or predict the release kinetics of a drug from the nanocarriers. Since the release study obtained in the case of MTF/TPA/nMCM-48 at pH 1.2 shows much slower release, and therefore, the release kinetics for the same was only carried out. Drug dissolution from the nanocarriers has been described by kinetic models in which the dissolved amount of drug (Q) is compared to the function of the test time (t). Some analytical definitions and kinetic models of Q *versus* t used in the present scenario are zero order, first order, and Higuchi, as shown in Table 5.[24,25,35–37]

Therefore, in terms of kinetics and mechanism, MTF release from the MTF/TPA/nMCM-48 system adheres to zero-order kinetics (Fig. 13) and the Higuchi model of diffusion.

3.5. Metformin and cancer: evidence from epidemiology

According to a significant body of epidemiological evidence, MTF may be a therapeutic agent for cancer patients. Numerous clinical trials on the anticancer activity of MTF are being conducted for the treatment of cancer. Epidemiological and basic investigations have shown that it may also prevent the development of various types of tumours. Metformin has demonstrated the ability to impede the growth of various tumour cells in both *in vitro* and *in vivo* experiments; however, the exact mechanism underlying this effect is still not well known. Currently, the antitumor effect of MTF is known to be primarily mediated by two major pathways.[6,38–40]

In order to prevent tumour cell growth, the first mechanism, the I/IGF pathway, may lower the amount of I/IGF-1 in the bloodstream and deactivate its downstream PI3K/Akt/mTOR signalling pathways. The second mechanism, the AMPK signalling pathway, may make it easier for metformin to interact with tumour cells directly by increasing AMPK and blocking mTOR downstream.

Table 5 Correlation coefficient values of different models[a]

		Zero order	First order	Higuchi
Sr. no.	Formulation	Equation with R^2 value	Equation with R^2 value	Equation with R^2 value
1	MTF/TPA/nMCM-48	$Q = K_0t$, 0.9957	$\ln(1 - Q) = -K_1t$, 0.9883	$Q = K_2t_{1/2}$, 0.9828

[a] Where Q is the fraction of drug release at time t and K_0, K_1, and K_H are the release apparent rate constants in each model.

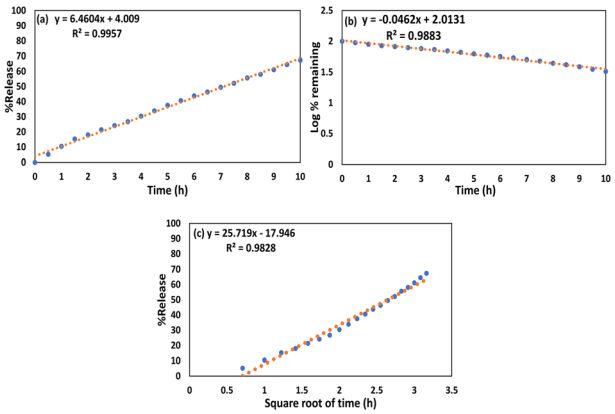

Fig. 13 Release kinetic model of MTF/TPA/nMCM-48: (a) zero order, (b) first order and (c) Higuchi model.

Therefore, it was deemed to be of interest to perform the *in vitro* cytotoxicity (MTT Assay) of the developed DDS, MTF/TPA/nMCM-48, and check its cytotoxicity, considering the anticancer potential of MTF.

3.5.1. Evaluation of *in vitro* cytotoxicity. Fig. 14 shows the % viability of HepG2 cells at different concentrations of MTF, TPA/nMCM-48, MTF/nMCM-48 and MTF/TPA/MCM-48. In the case of the pure drug and carrier, at a concentration ranging from 25 to 500 μg mL^{-1}, no such observable change in the % cell viability could be seen. In the case of MTF/nMCM-48, at a concentration ranging from 25 to 500 μg mL^{-1}, %cell death could be seen and ≤10% cell death could be observed at the highest concentration (200 μg mL^{-1}). However, MTF/TPA/nMCM-48 clearly showed a decline in cell viability (70.3%), with the highest percentage of cell death occurring at 250 μg mL^{-1}. As expected, MTF/TPA/nMCM-48 was shown to be more toxic to cancer cells than MTF/nMCM-48. The results obtained from the assay are noteworthy, as they demonstrate that MTF/TPA/nMCM-48 exhibited cytotoxicity towards HepG2 cells. Therefore, the results obtained support the use of the developed DDS against individuals with DMT2, who are at an increased risk of developing cancer.

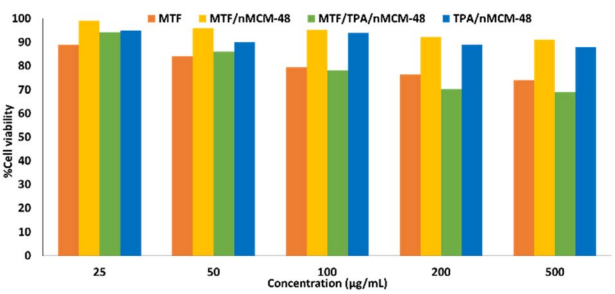

Fig. 14 Cytotoxicity assessment at different concentrations.

4. Conclusions

To summarise, for the first time, we reported the development of nMCM-48 functionalized with an inorganic moiety for the controlled release of MTF in order to address the shortcomings of the drug. MTF/TPA/nMCM-48 release profiles are compared to those of Glycomet-250 (marketed drug), and the results demonstrated that the new system is superior and exhibits more ordered and regulated release. Release profiles showed that much controlled release was obtained in SGF, and TPA acts more effectively as a functionalizing agent than a capping agent as well as MTF release follows the zero-order release kinetics followed by Higuchi model of diffusion according to the kinetic study. Further, taking into account the anticancer potential of MTF, the MTT assay using HepG2 cells showed a significant decrease in % cell viability, and therefore, the designed drug delivery system can be used to treat diabetic patients with genetic history of malignancy. Thus, the developed DDS offers a new and better approach of delivering MTF, thus encouraging further development of this formulation, which could be beneficial for treating both antidiabetic and anticancer patients.

Author contributions

Anjali Patel: conceptualization, methodology, writing – review & editing, supervision. Debatrayee Dasgupta: investigation, formal analysis, writing – original draft.

Conflicts of interest

There are no conflicts to declare.

Data availability

The authors declare that all the data will be made available upon reasonable request.

Acknowledgements

AP and DD are thankful to the Department of Chemistry, The Maharaja Sayajirao University of Baroda for TG-DTA analysis.

DD is thankful to SHODH (Scheme of Developing High Quality Research, KCG/SHODH/2022–23/) for providing the financial support.

References

1 R. A. Khan, N. Patel, A. Folajimi, B. R. Bai, V. Patel, P. K. Komminni, S. K. Palleti and S. Hirani, *Cureus*, 2023, **15**, e35014.
2 R. Wiwattanapatapee, K. Klabklay, N. Raksajit, W. Siripruekpong, N. Leelakanok and A. Petchsomrit, *Heliyon*, 2023, **9**, e14796.
3 S. Dutta, R. B. Shah, S. Singhal, S. Bansal, S. Sinha, M. Haque and S. B. Dutta, *Drug Des. Devel. Ther.*, 2023, **17**, 1907–1932.
4 U. Smith and E. A. M. Gale, *Diabetologia*, 2010, **53**, 1541–1544.
5 M. Ghosh, S. Mandal, S. Paul, S. Chakrabarty, R. Anindita, C. Gopal and P. S. Kumar, *J. Drug Deliv. Sci. Technol.*, 2023, **87**, 104781.
6 Y. Hua, Y. Zheng, Y. Yao, R. Jia, S. Ge and A. Zhuang, *J. Transl. Med.*, 2023, **21**, 1–20.
7 Y. Du, Y. J. Zhu, Y. X. Zhou, J. Ding and J. Y. Liu, *Mol. Biomed.*, 2022, **3**, 1–32.
8 Y. C. Chen, H. Li and J. Wang, *Am. J. Transl. Res.*, 2020, **12**, 4885–4901.
9 D. R. Morales and A. D. Morris, *Annu. Rev. Med.*, 2015, **66**, 17–29.
10 S. Noreen, S. Hasan, S. A. Ghumman, S. Anwar, H. Y. Gondal, F. Batool and S. Noureen, *ACS Omega*, 2023, **8**, 5925–5938.
11 M. Hu, T. Gou, Y. Chen, M. Xu, R. Chen, T. Zhou, J. Liu, C. Peng and Q. Ye, *Molecules*, 2023, **28**, 2471–2484.
12 M. Dadashpour, H. Mahmoudi, Z. Rahimi, R. J. Poodeh, H. Mousazadeh, A. Firouzi Amandi, Y. Yazdani, A. N. Asl and A. Akbarzadeh, *J. Drug. Deliv. Sci. Technol.*, 2023, **87**, 104769.
13 F. Zhang, W. Liu, Y. Long and H. Peng, *Appl. Biochem. Biotechnol.*, 2023, **195**, 4067–4083.
14 H. S. Nouri, A. Jafari, L. Roshangar, M. Dadashpour, Y. P. Soltanahmadi and N. Zarghami, *Mater. Sci. Eng. C.*, 2020, **116**, 111225.
15 N. Naseri, E. Ajorlou, F. Asghari and Y. P. Soltanahmadi, *Artif. Cells Nanomed. Biotechnol.*, 2018, **46**, 1111–1121.
16 S. Samadzadeh, M. Babazadeh, N. Zarghami, Y. Pilehvar-Soltanahmadi and H. Mousazadeh, *Mater. Sci. Eng. C.*, 2021, **118**, 111384.
17 S. Mashayekhi, S. Rasoulpoor, S. Shabani, N. Esmaeilizadeh, H. Serati-Nouri, R. Sheervalilou and Y. Pilehvar-Soltanahmadi, *Int. J. Pharm.*, 2020, **587**, 119656.
18 T. Li, S. Shi, S. Goel, X. Shen, X. Xie, Z. Chen, H. Zhang, S. Li, X. Qin, H. Yang, C. Wu and Y. Liu, *Acta Biomater.*, 2019, **89**, 1–13.
19 A. M. Escobar, G. Blustein, R. Luque and G. P. Romanelli, *Catalysts*, 2021, **11**, 291.
20 B. Hasenknopf, *Front. Biosci.*, 2005, **10**, 275–287.
21 F. Carvalho and M. Aureliano, *Int. J. Mol. Sci.*, 2023, **24**, 5043.
22 M. B. Čolović, M. Lacković, J. Lalatović, A. S. Mougharbel, U. Kortz and D. Z. Krstić, *Curr. Med. Chem.*, 2019, **27**, 362–379.
23 Z. Ilyas, H. S. Shah, R. Al-Oweini, U. Kortz and J. Iqbal, *Metallomics*, 2014, **6**, 1521–1526.
24 D. Dasgupta and A. Patel, *Mater. Adv.*, 2022, **3**, 8220–8228.
25 D. Dasgupta, M. Das, S. Thakore, A. Patel, S. Kumar and S. Seshadri, *J. Drug Deliv. Sci. Technol.*, 2022, **72**, 103419.
26 T. Mosmann, *J. Immunol. Methods*, 1983, **65**, 55–63.
27 S. C. Jagdale, S. A. Patil, B. S. Kuchekar and A. R. Chabukswar, *J. Young Pharm.*, 2011, **3**, 197–204.
28 M. S. Refat, F. M. Al-Azab, H. M. A. Al-Maydama, R. R. Amin, Y. M. S. Jamil and M. I. Kobeasy, *Spectrochim. Acta A Mol. Biomol. Spectrosc.*, 2015, **142**, 392–404.
29 H. P. Boehm, *Discuss. Faraday Soc.*, 1971, **52**, 264–275.
30 J. P. Cloarec, C. Chevalier, J. Genest, J. Beauvais, H. Chamas, Y. Chevolot, T. Baron and A. Souifi, *Nanotechnology*, 2016, **27**, 295602.
31 A. V. Stuart, Y. Clement, P. Sealy, R. Löbenberg, L. Montane-Jaime, R. G. Maharaj and A. Maxwell, *Dissolut. Technol.*, 2015, **22**, 17–21.
32 V. Kumar, A. Joshi, K. Kumar, D. Teotia, A. S. Ikram, D. Khairya and I. J. Indig, *Herbs Drugs*, 2022, **7**, 99–104.
33 R. Uddin, N. Saffoon, K. Bishwajit Sutradhar and I. J. Cur, *Biomed. Phar. Res.*, 2011, **1**, 201–207.
34 A. Ravindran Chandrasekaran, C. Yoke Jia, C. Sheau Theng, T. Muniandy, S. Muralidharan and S. Arumugam Dhanaraj, *J Appl Pharm Sci*, 2011, 214–217.
35 S. Adhikary, A. Al Hoque, M. Ray, S. Paul, A. Hossain, S. Goswami and R. Dey, *Appl. Biochem. Biotechnol.*, 2023, **195**, 4712–4727.
36 M. M. Abdul Hameed, S. A. P. Mohamed Khan, B. M. Thamer, N. Rajkumar, H. El-Hamshary and M. El-Newehy, *Polym. Adv. Technol.*, 2022, 1–18.
37 M. V. S. Varma, A. M. Kaushal, A. Garg and S. Garg, *Am. J. Drug Deliv.*, 2004, **2**, 43–57.
38 F. Zi, H. Zi, Y. Li, J. He, Q. Shi and Z. Cai, *Oncol. Lett.*, 2018, **15**, 683–690.
39 P. Saraei, I. Asadi, M. A. Kakar and N. Moradi-Kor, *Cancer Manage. Res.*, 2019, **11**, 3295–3313.
40 M. Daugan, A. D. Wojcicki, B. d'Hayer and V. Boudy, *Pharmacol. Res.*, 2016, **113**, 675–685.